

Experimental Study on Structural Performance of Precast CES Shear Walls

Tomoya Matsui

Toyohashi University of Technology, Japan

Suguru Suzuki

Graduate School of Engineering, Osaka University, Japan

Hiroshi Kuramoto

Osaka University, Japan



SUMMARY:

The objective of this study is to develop the CES shear wall in composite Concrete Encased Steel (CES) structures composed of steel and fiber reinforced concrete, and Static loading tests were conducted on the two shear wall with a simplified anchoring method for connecting the CES frame to the FRC wall panel including one precast shear wall specimen. This paper describes the summary and investigates the failure mode, ultimate strength and restoring force characteristics. As the result, it was observed that the shear strength was not so influenced by simplifying the anchorage of wall reinforcing bars to CES beam and column. The deformability of CES shear wall slightly improves by omitting anchorage of wall reinforcing bars. The Significant slip deformation between the wall panel and CES frame was observed in precasted CES shear wall.

Keywords: Composite structure, CES shear wall, Fiber reinforced concrete, Precast wall, Anchorage method

1. INTRODUCTION

Steel Reinforced Concrete (SRC) Structures developed in Japan have good structural performance for resisting lateral forces imposed by wind and earthquakes, and have been adopted for medium-rise, high-rise, and super high-rise buildings. However, the number of SRC buildings constructed has decreased since the 1990s. Although the decrease might be caused by the development of a new structural engineering system called the High-strength concrete structure or Concrete-Filled Steel Tube (CFT) structure, the main reason seems to be the construction problems that increase construction costs and lengthen construction schedules. Even so, it could be important that SRC structures provide better seismic performance in comparison with other structural systems. So, the authors aim to develop a structural system with as good seismic performance as SRC structures and good workability, and have conducted a continuing development study on composite Concrete Encased Steel (CES) structures composed of steel and fiber reinforced concrete (FRC) as shown in Figure 1.1.

In the experimental study on CES columns, CES beam-column joints, and a two-bay two-story CES frame, it was confirmed that the CES structural system showed stable restoring force characteristics and good seismic performance.

On the other hand, a shear wall, which is a main earthquake resistant member, is also effective at increasing the stiffness and strength of the CES structural system. However, it will be difficult to arrange wall reinforcing bars in the CES structure, which contains encased steel in beams and columns. Recently, there have been some researches on

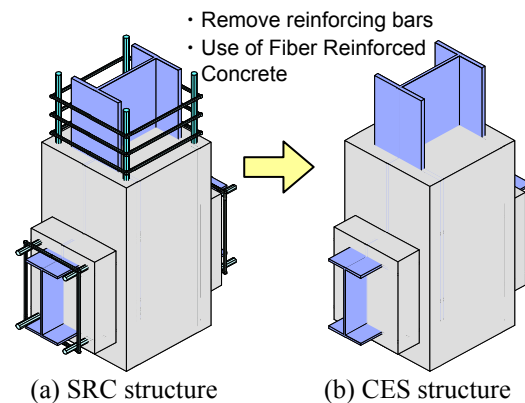


Figure 1.1. Composite Concrete Encased Steel structural system

methods of joining a frame and wall panel in SRC shear walls. It is likewise an important problem to improve the workability of a frame and wall panel joint in the CES structure.

Because of these backgrounds, static loading tests were carried out on CES shear walls with different anchorage methods for the CES frame and FRC wall panel, and the basic structural performance, such as strengths, deformability and failure modes, of the CES shear walls were investigated by the authors. As the results, it was confirmed that the effect of anchorage condition of wall longitudinal reinforcement on shear strength and flexural strength of CES shear wall is small. In addition the deformability of CES shear wall slightly improves by omitting anchorage of wall longitudinal reinforcement.

Therefore, in the term of rationalization and laborsaving of construction, omission of anchorage of transverse wall reinforcing bars and applicability to precast method are considered as the next subjects. In this study, Static loading tests were conducted on the two shear wall with a simplified anchoring method for connecting the CES frame to the FRC wall panel including one precast shear wall specimen. This paper describes the summary and investigates the failure mode, ultimate strength and restoring force characteristics.

2. OUTLINE OF CES SHEAR WALL TESTS

2.1. Description of Specimens

The specimens are designed to simulate the lower two story of multi-story shear wall in medium-high-rise building and scaled to one-third of the prototype walls. Two specimens were prepared in this test. Specimen CWDS was normal type, Specimen CWPS was precast type dividing FRC panel into two parts each story. Configuration and bar arrangement of specimens are shown Figure 2.1. and Figure 2.2. Detail of the section is shown in Table 2.1. The column had a 250 mm square cross-section, and the beam section was 200 mm × 250 mm. The column span length was 1,800 mm, and the wall thickness was 100 mm.

The longitudinal and transverse wall reinforcing bars for Specimen CWDS were not anchored to CES frame and bent at a 180° hook in the wall panel. The top and bottom of transverse wall reinforcing bars at a story were securely fixed by welding to the steel web in the CES columns in order to fix reinforcing bars on work as shown Figure 2.2. As for Specimen CWPS, CES frame was made in first. Then, precast wall panel was set, and the transverse reinforcing bars of the precast wall panel were welded. Non-shrinkage mortar was injected into the spaces between the precast wall panel and the CES frame. In addition, the precast wall panel had shear cotter at the edge of that.

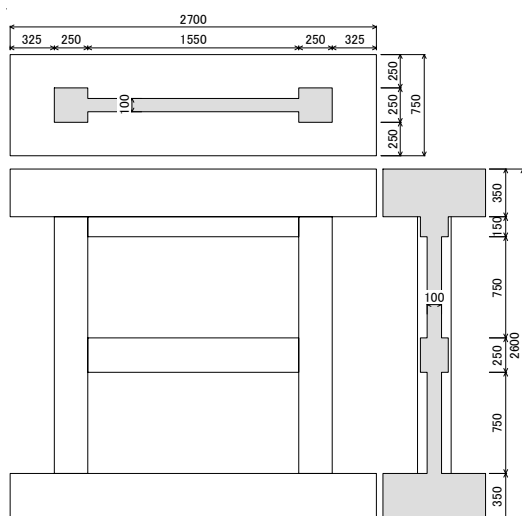


Figure 2.1. Specimen configuration

Table 2.1. Specification of section

Specimen	CWDS	CWPS	
Column	B×D	250×250 (mm)	
	Steel	H-170×120×6×9 ($s_p=4.9\%$)	
Beam	b×D	200×250 (mm)	
	Steel	H-148×100×6×9 ($s_p=5.2\%$)	
Wall	Thickness	100 (mm)	
	Longitudinal bar	D6@75 zigzag ($w_p=0.42\%$)	D6@65 zigzag ($w_p=0.42\%$)
	Transverse bar		

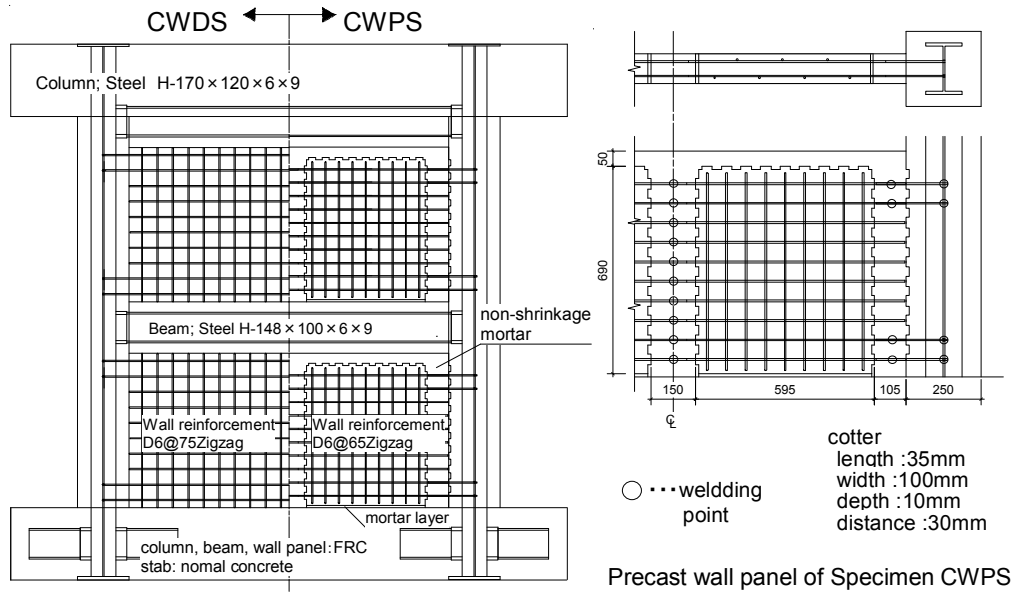


Figure 2.2. Bar arrangement

Table 2.2. Material properties of concrete

Specimen		σ_B (MPa)	E_c (GPa)	ϵ_{c0} (μ)	Age (day)
CWDS	1 story	30.3	22.1	2619	112
	2 story	33.7	25.6	2337	106
CWPS	1 story	29.0	23.0	2493	118
	2 story	33.8	24.7	2506	112

σ_B : Compressive strength, E_c : Elastic modulus, ϵ_{c0} : Strain at compressive strength

Table 2.3. Material properties of mortar

CWPS		σ_B (MPa)
Mortar layer	Under wall panel	29.6
Non-shrinkage mortar	Vertical and transverse joint area	92.5

Table 2.4. Material properties of steel.

	Yield strength (MPa)	Tensile strength (MPa)	Elastic modulus (GPa)
PL-6 (SS400) column	300	422	197
PL-9 (SS400) column	297	442	209
PL-6 (SS400) beam	317	---	---
PL-9 (SS400) beam	338	---	---
D6 (SD295A)	396	518	192

Shear span ratio was 1.1 in both specimens, and Specimen CWDS was expected to be shear failure. Furthermore, results of specimen CWAS that reported previously are also shown in chapter on test results. Although Specimen CWAS was almost identical with Specimen CWDS, all transverse wall reinforcing bar was welded to steel web in the CES column.

The mechanical properties of the concrete, mortar and steel used are shown in Tables 2.2., 2.3. and 2.4., respectively. Vinylon fibers with a diameter of 0.66 mm and a length of 30 mm were used for the FRC. The volumetric ratio of the fibers was 1.0%, and the water-cement ratio was 60%.

2.2. Loading Program

Figure 5 shows the loading apparatus used. The wall specimens were loaded with horizontal cyclic shear forces using a hydraulic jack with a 2,000 kN capacity, while applying a constant axial force of 1,086 kN ($N/N_0 = 0.2$, N : axial load, N_0 : axial load capacity including steel of columns) using two vertical manual jacks, each of which had a 2,000 kN capacity. During the testing, additional moment was also applied to the top of the specimens using vertical jacks to maintain the prescribed shear-span ratio of 1.1, using the following equations.

$$N_e = \frac{N_c}{2} - \frac{Q}{l}(h-a), \quad N_w = \frac{N_c}{2} + \frac{Q}{l}(h-a) \quad (2.1)$$

where N_e : axial force of east side jack, N_w : axial force of west side jack, N_c : constant axial force (1,086 kN), Q : shear force, l : distance between two vertical jack, h : assumed height of applied shear force, and a : actual height of applied shear force.

The loading was conducted by controlling the relative wall drift angle, R , given by the ratio of the height corresponding to the measuring point for the horizontal displacement at the top of the specimen, h_o , (2,050 mm), to the horizontal deformation, δ , i.e., $R = \delta/h_o$. The horizontal load sequence consisted of two cycles for each story drift angle.

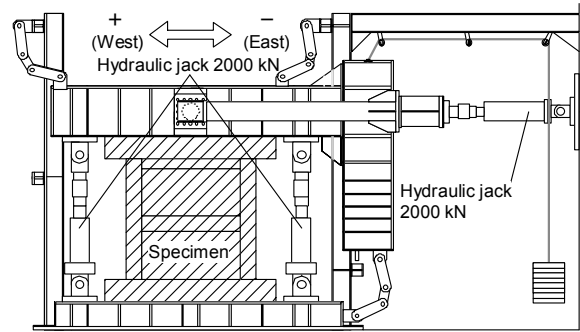


Figure 2.4. Loading apparatus

2.3. Measuring Method

In the tests, the horizontal displacement was measured, along with the longitudinal deformation of the column and partial deformation of the wall panel. The strains on the steel of the column and beam, and on the longitudinal and horizontal bars of the wall, were measured using strain gages. Additionally, the widths of cracks were measured using a crack scale at each loading cycle.

3. TEST RESULTS

3.1. Failure Mode

Figure 3.1. shows the cracking pattern of each specimen at the drift angle of 0.75×10^{-2} rad. and after final loading cycles. In Specimen CWDS, shear crack at the first story wall panel and flexural crack at the boundary column occurred in the cycle of 6.25×10^{-4} rad. Then, slip was observed at the underside

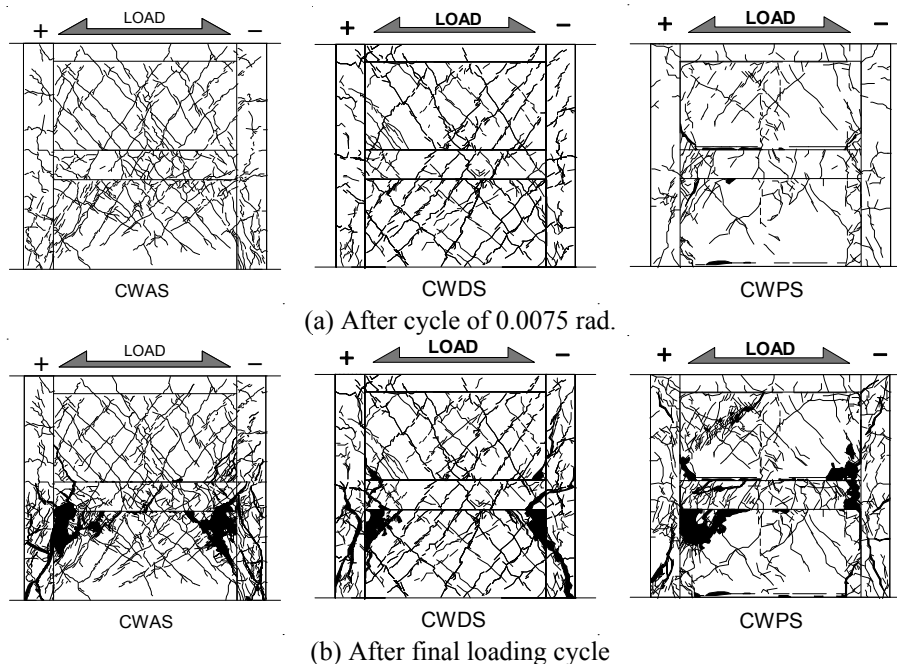


Figure 3.1. Cracking patterns

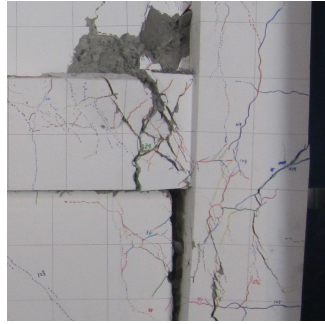


Photo 3.1. Damage of Specimen CWPS at drift angle of -0.03rad .



Photo 3.2. Fracture of steel beam of Specimen CWPS (Observation after test)

of beam in the cycle of $0.5 \times 10^{-2}\text{rad}$. The maximum shear force reached at the drift angle of $0.75 \times 10^{-2}\text{rad}$, and shear cracks spread at the upper corner of the first-story wall and the lower corner of the second-story wall. After maximum shear, spread shear crack and compressive failure of concrete at the upper corner of the first-story wall and the lower corner of the second-story wall developed with increase of loading cycle, and damage of concrete at the boundary column increased, the loading finished at the drift angle of $5.0 \times 10^{-2}\text{rad}$.

As for Specimen CWPS, crack at the area of non-shrinkage mortar and flexural crack at the column occurred in the cycle of $6.25 \times 10^{-4}\text{rad}$. Then, slip was observed at the underside of beam and at the boundary of column and mortar in the cycle of $0.25 \times 10^{-2}\text{rad}$. The shear cracks spread at the upper corner of the first-story wall and the lower corner of the second-story wall in the cycle of $0.5 \times 10^{-2}\text{rad}$. After the maximum shear force reached at the drift angle of $1.5 \times 10^{-2}\text{rad}$, damage of concrete at the column, beam and corner of wall increased with increase of loading cycle. In addition, separation at the boundary of column and mortar is severe as shown in Photo 3.1., and steel of the beam fractured at the end in the loading cycle of $5.0 \times 10^{-2}\text{rad}$ as shown in Photo 3.2.

3.2. Hysteretic Characteristics

Figure 3.2. shows the shear force versus drift angle relationships. Specimen CWDS recorded maximum shear force of 1,204 kN at the drift angle of $0.75 \times 10^{-2}\text{rad}$. After that, shear forces of Specimen CWDS decreased slowly with damage of concrete of wall panel and column. Specimen CWPS recorded maximum shear force of 995 kN at the drift angle of $1.5 \times 10^{-2}\text{rad}$, maximum shear force of Specimen CWPS was about 20 percent less than that of Specimen CWDS. After maximum shear force, Specimen CWPS maintained shear force. Then, Specimen CWPS showed strength deterioration at the drift angle of $3.5 \times 10^{-2}\text{rad}$ with fracture at the end of steel of the beam. Restoring characteristics of Specimen CWPS was different from that of Specimen CWDS.

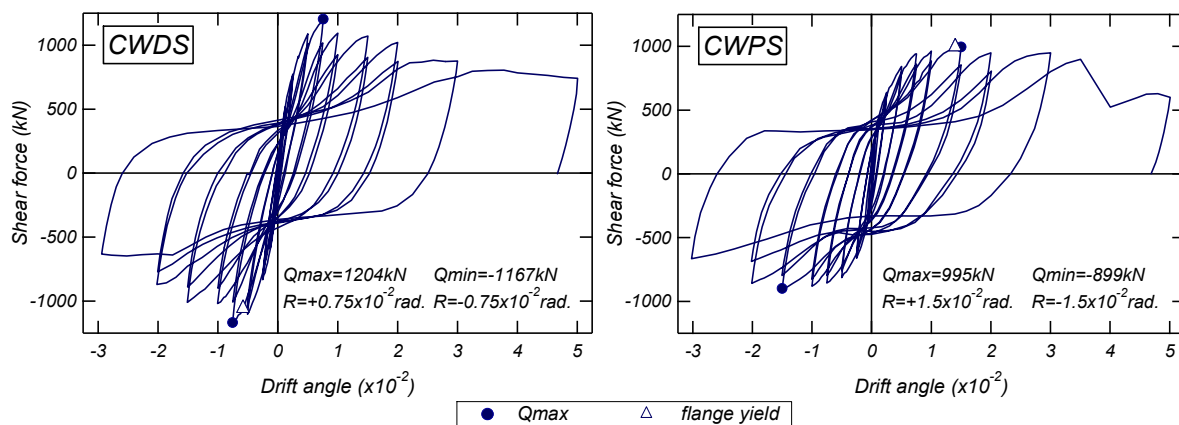


Figure3.2. Shear force versus drift angle relationships

Figure 3.3. shows envelope curve of the specimens including Specimen CWAS. Shear strength of Specimen CWDS reduced anchorage of transverse wall reinforcing bars was smaller than that of Specimen CWAS. It is thought that this discrepancy was caused by difference of compressive strength of concrete and shear strength of Specimen CWDS was as large as shear strength of Specimen CWAS. But, it is confirmed that slop of strength deterioration of Specimen CWDS is gentler than that of Specimen CWAS after maximum shear force. It is thought that these different strength deterioration is caused by the slip under the beam of Specimen CWDS was larger than that of Specimen CWAS (refer to Section 3.4. on Slip and Separation at the Boundary of Wall Panel and CES Frame). Therefore, it could be said that the damaged concrete area of the wall panel in Specimen CWDS was smaller than Specimen CWAS as shown Figure 3.1. In addition, both specimens showed strength deterioration after maximum shear force, it is thought that shear strength was determined by failure of concrete of wall panel. However, maximum shear force of CWPS was about 20 % less than that of CWDS, it is thought that failure mode of Specimen CWPS formed failure mode with slip at the boundary of wall panel and CES frame.

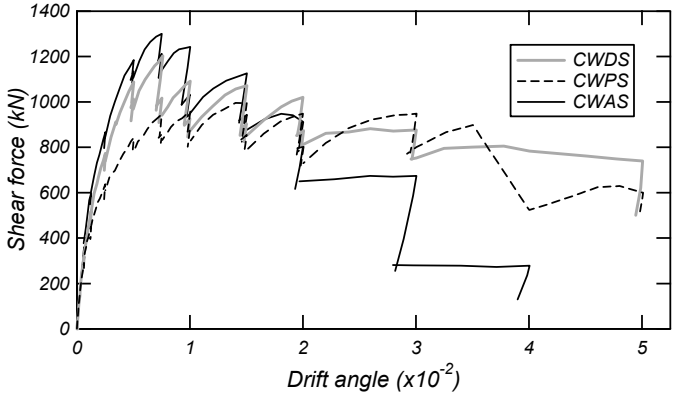


Figure 3.3. Envelope curve of shear force versus drift angle relationships

3.3. Cumulative Dissipated Energy

Figure 3.4. shows cumulative dissipated energy of specimens at each loading cycle. Result of Specimen CWAS is until cycle of 3.0×10^{-2} rad. Cumulative dissipated energy is calculated by cumulate area of each hysteresis loop in Shear force versus drift angle relationships. Cumulative dissipated energy of Specimen CWDS was the largest, Specimen CWPS and Specimen CWAS, in that order at final loading cycle. However, the difference of cumulative dissipated energy until the loading cycle of 3.0×10^{-2} rad. was about 3 % in three specimens, and it is found that three specimens showed almost the same level of energy dissipation performance.

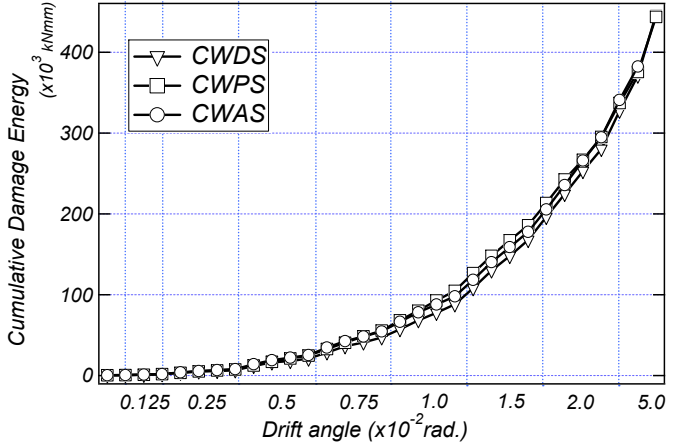


Figure 3.4. Cumulative dissipated energy of CES shear walls

3.4. Slip and Separation at the Boundary of Wall Panel and CES Frame

Figure 3.5. shows slip displacement and separation displacement at the boundary of wall panel and beam at the peak of positive loading until drift angle of 1.5×10^{-2} rad. Seeing slip displacement at the boundary of wall panel and beam, slip in specimen CWPS occurred at the drift angle of 0.25×10^{-2} rad., slip in specimen CWDS occurred at the drift angle of 0.5×10^{-2} rad. and slip in specimen CWAS occurred at the drift angle of 1.0×10^{-2} rad. In addition, seeing slip displacement between wall panel and boundary column, it is found that slip of Specimen CWPS was larger than that of Specimen CWDS. Slip at the boundary of wall panel and CES frame tends to occur in specimen CWPS, CWDS and CWAS, in that order.

On the other hand, it is observed that separation at the boundary of wall panel and column began to occur at the drift angle of 0.25×10^{-2} rad. in the specimen CWPS. Then, deformation behavior and failure behavior as shown in Figure 3.7. appear with increase of drift angle. Because of the separation at the boundary of wall panel and column or spreading shear crack at the corner of wall panel along with slip at the boundary of wall panel and beam significantly occur, CES shear wall move to a separation between the column on compressive side and the column on tensile side and wall panel, and the each member deforms individually.

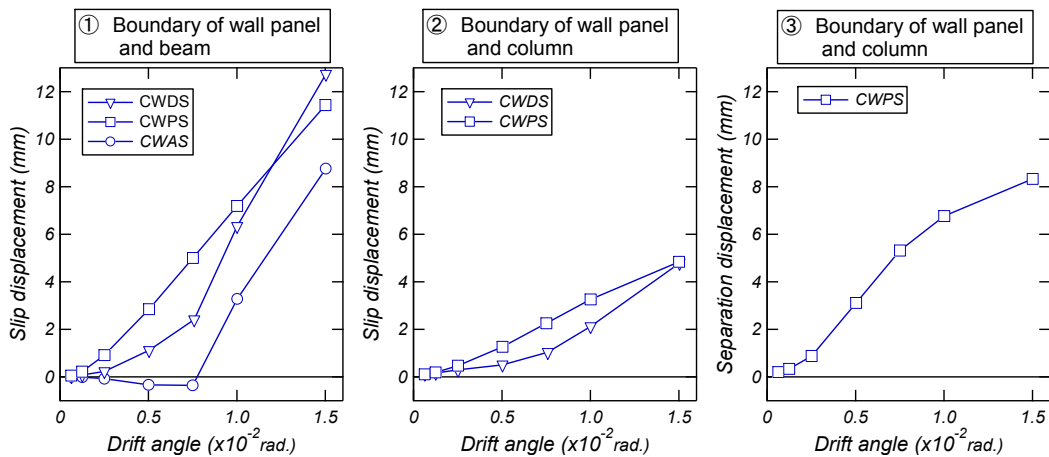


Figure 3.5. Slip and separation at the boundary of wall panel and CES frame

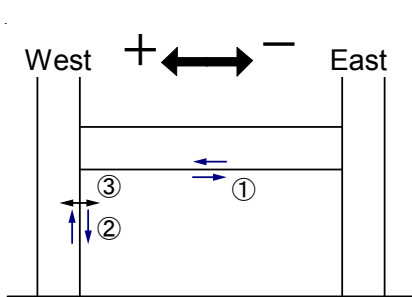


Figure 3.6. Measured point of boundary

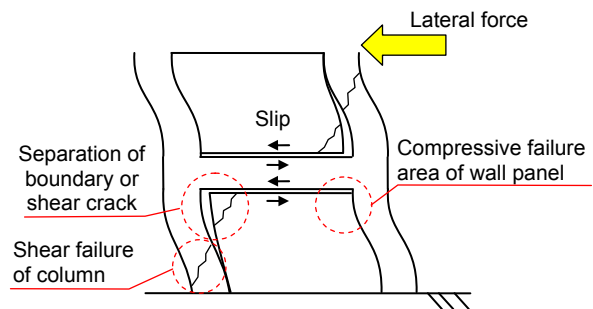


Figure 3.7. Deformation behaviour of Specimen CWPS of Precasted CES shear wall

3.5. Deformation Components

Figure 3.8. shows the percentage of shear deformation and bending deformation at the peak of positive loading cycle until the drift angle of 2.0×10^{-2} rad. for all specimens. The bending deformation was calculated using curvature obtained from vertical displacement measured at the side column. Shear deformation was calculated by subtract bending deformation from total deformation.

As for all specimens, shear deformation was larger than bending deformation, and shear deformation increased with increasing drift angle. Shear deformation of Specimen CWDS whose anchorage of transverse wall reinforcing bars was reduced was larger than that of Specimen CWAS. And Shear deformation of Specimen CWPS that was precasted CES shear wall was larger than Specimen CWDS. The more slip displacement, the larger percentage of shear deformation, and the effect of slip behavior is conformed in component of deformation of CES shear wall.

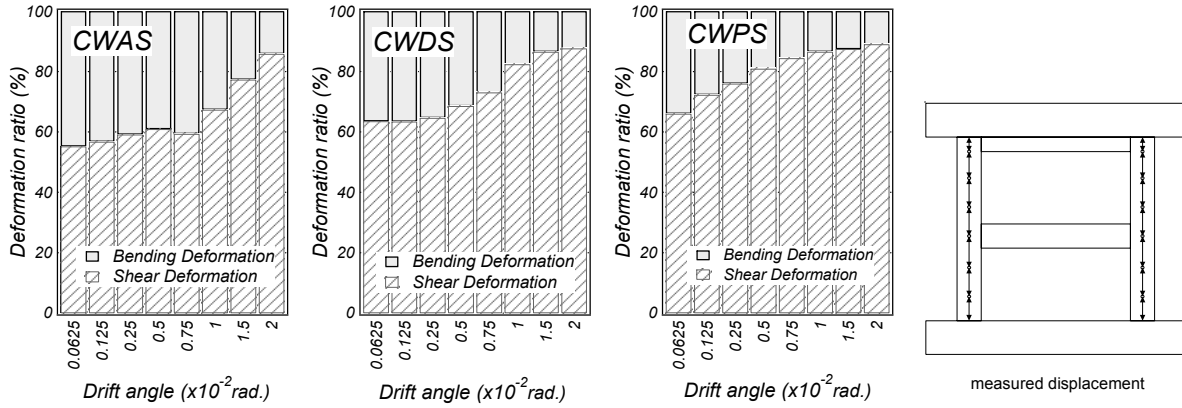


Figure 3.8. Percentage of deformation components

4. EVALUATION OF ULTIMATE STRENGTH

The results of calculations for the ultimate strengths of the specimens are shown in Table 4.1. The flexural strength was calculated using Eqn. 4.1, which does not contain a term for the reinforcing bars in a boundary column from an equation based on the “AIJ Standard for Structural Calculation of Steel Reinforced Concrete Structures”. Moreover, the longitudinal wall reinforcing bars were not considered in calculations, $m_w A = 0$. The shear strength was calculated using Hirosawa’s Equation (Eqn. 4.2) for reinforced concrete shear wall and the Truss-Arch Equation (Eqn. 4.4). In the Truss-Arch Equation, it is thought that the flexural capacity of a CES boundary column contributes to the shear strength of a CES shear wall, which is expressed by Eqn. 4.5. Because it was observed that the steel flange of the beam yielded at the maximum shear force in the test, the shear strength was calculated by adding the lower steel flange of the beam to the transverse wall reinforcing bar, as shown in Eqn. 4.3 and Eqn. 4.8.

-Flexural strength

$$Q_{mu} = \left(\frac{N}{2} + {}_{sCS}A_s \sigma_y + \frac{m_w A}{2} \sigma_y \right) l_w / h_w \quad (4.1)$$

-Shear strength by Hirosawa’s equation

$$Q_{su1} = \left[\frac{0.068 p_{te}^{0.23} \cdot (F_c + 18)}{\sqrt{M/(Q \cdot l) + 0.12}} + 0.85 \sqrt{\sigma_{wh} \cdot p_{wh}} + 0.1 \sigma_0 \right] \cdot t_e \cdot j \quad (4.2)$$

$$p_{wh} = \frac{a_h}{b_e \cdot s} + \frac{a_f}{b_e \cdot h'} \cdot \frac{\sigma_{fy}}{\sigma_{wy}} \quad (4.3)$$

-Shear strength by Truss-Arch equation

$$Q_{su2} = w t \left\{ w l_t \cdot p_{se} \cdot \sigma_{wh} \cot \phi + \tan \theta (1 - \beta) w l_a \cdot v \cdot \frac{c \sigma_B}{2} \right\} \quad (4.4)$$

$$w l_a = l_w + \frac{1}{\cos \theta} \sqrt{\frac{2 {}_{CS} M_U}{v \cdot \sigma_B \cdot w t (1 - \beta)}} \quad (4.5)$$

$$\beta = \frac{2 w p \sigma_{wh}}{v c \sigma_B} \quad (4.6)$$

$$\tan \theta = \sqrt{\left(\frac{h_w}{wl + D}\right)^2 + 1} - \frac{h_w}{wl + D} \quad (4.7)$$

$$p_{se} = wp + \frac{a_f \cdot \sigma_{fy}}{wt \cdot h' \cdot \sigma_{wh}} \quad (4.8)$$

Where N : total axial force in the boundary columns (N); $s_c A_s$, $m_w A_s$: cross sectional areas of the steel in a boundary column and the vertical reinforcing bars in the wall, respectively; $s \sigma_y$, $w \sigma_y$: yield strengths of the steel of a boundary column and the vertical reinforcing bars in the wall, respectively (N/mm^2); l_w : distance between the centers of the boundary columns of the wall; h_w : assumed height of applied lateral force; p_{le} : equivalent tensile reinforcement ratio (%); l : wall length; t_e : equivalent thickness of wall; j : distance between the centroid of tension and compression force; p_{wh} : equivalent lateral reinforcing ratio; σ_{wh} : yield strengths of the lateral reinforcing bar (N/mm^2); σ_0 : axial stress (N/mm^2); M/Q : shear span; h' : floor height; F_c , $c \sigma_B$: compressive strength of concrete (N/mm^2); a_f : cross sectional area of the steel flange in the boundary beam; σ_{fy} : yield strength of the steel flange in the boundary beam; wt : thickness of wall; wl_t : equivalent wall length of truss mechanism ($=l$); p_{se} : lateral reinforcing ratio; wp : wall lateral reinforcing ratio; ϕ : angle of concrete strut of truss mechanism ($\cot \phi = 1$); θ : angle of concrete strut of arch mechanism; v : effective coefficient of concrete; wl_a : equivalent wall length of arch mechanism; and $c_s M_{Uj}$: ultimate flexural moment of boundary column.

Table 4.1. Calculated strength and measured strength

Specimen		CWAS	CWDS	CWPS	
Measured strength		Q_{exp} (kN)	1300	1204	995
Flexural strength		Q_{mu} (kN)	1178	1164	1164
Shear strength	Hirosawa's Eqn.	Q_{su1} (kN)	1269 (1.02)	1142 (1.05)	1123 (0.89)
	Truss-Arch Eqn.	Q_{su2} (kN)	1319 (0.99)	1222 (0.99)	1202 (0.83)

Compressive strength of concrete at 1st story is used in calculation.

Figures in parenthesis are ratio of measured strength to calculated strength

As for Specimen CWAS and CWDS, which showed shear failure, the ratios of measured strength to calculated strength are about 0.99 to 1.05. The calculated strengths show good agreement with the experimental results in both equations, and even if anchorage of wall reinforcing bars is omitted, it is found that shear strength of CES shear wall could be evaluated by Eqn. 4.2. and Eqn. 4.4.

As for Specimen CWPS which is the precast shear wall, the ratios of measured strength to calculated strength are about 0.81 to 0.89, and these equation overestimate shear strength of specimen CWPS. Because it is thought that Specimen CWPS formed different failure mechanism from other specimens, it is necessary to examine the different evaluation method.

5. CONCLUSIONS

Static loading tests were conducted on the two shear wall with a simplified anchoring method for connecting the CES frame to the FRC wall panel including one precast shear wall specimen. The failure mode, lateral load carrying capacity, and deformability of CES shear walls were examined. The following conclusions can be drawn.

- (1) The shear strengths are almost the same level between Specimen CWDS that transverse and longitudinal wall reinforcement anchorage was reduced and Specimen CWAS that just longitudinal wall reinforcement anchorage was reduced.

(2) The deformability of a CES shear wall improves by omitting the anchorage for the transverse wall reinforcement. This was because the damaged area of concrete for the wall panel was reduced by the occurrence of slip at the boundary of wall panel and CES frame because of the omission of anchorage for the wall reinforcement.

(3) Although damage of concrete at the corner of wall panel and column were finally significant for each specimen, Specimen CWPS of precasted CES shear wall showed slip at the boundary of wall panel and CES frame at the small level of drift angle, and it is thought that slip deformation affect failure mode in precasted CES shear wall.

(4) Although Shear strength of specimen CWPS of precasted CES shear wall was smaller than that of Specimen CWDS, Cumulative dissipated energy of Specimen CWPS was about the same as that of other specimen.

(5) The shear strength of CES shear wall with a simplified anchoring method for connecting the CES frame to the wall panel could be evaluated using Hirosawa's Equation and Truss-Arch Equation, however, further investigation on the different evaluation method is necessary for Precast CES shear wall.

REFERENCES

- Fauzan, Kuramoto, H. Matsui, T. and Taguchi, T. (2008). Test on 2-Bay 2-Story CES Frame Subjected to Lateral Load Reversals, *Proceedings of Fourteenth World Conference on Earthquake Engineering*. Paper No. 05-06-0063.
- Matsui, T. and Kuramoto, H. (2008). Stress Transferring Mechanism of Beam-Column Joints for Composite CES Structural System Subjected to Seismic Load. *Proceedings of Fourteenth World Conference on Earthquake Engineering*. Paper No. 05-06-0081.
- Fujimoto, T. Kuramoto, H. and Matsui, T. (2008). Seismic Performance of Columns and Beam-Column Joints in Composite CES Structural System. *Proceedings of Fourteenth World Conference on Earthquake Engineering*. Paper No. 05-06-0073
- Matsui, T. Kuramoto, H. (2011). A fundamental study on structural performance of CES Shear Walls with Different Anchorage Condition of Wall Reinforcement. *8th International Conference on Urban Earthquake Engineering proceedings*. 843-850.
- Architectural Institute of Japan. (2001). Standard for Structural Calculation of Steel Reinforced Concrete Structures. Architectural Institute of Japan. (in Japanese)